The cytosolic chaperone α-crystallin B rescues folding and compartmentalization of misfolded multispan transmembrane proteins

Massimo D'Agostino[1], Valentina Lemma[1,*], Giancarlo Chesi[2,*], Mariano Stornaiuolo[1], Magda Cannata Serio[1], Chiara D'Ambrosio[3], Andrea Scaloni[3], Roman Polishchuk[2,‡] and Stefano Bonatti[1,‡]

[1]Department of Molecular Medicine and Medical Biotechnology, University of Naples Federico II, 80131 Naples, Italy
[2]Telethon Institute of Genetics and Medicine (TIGEM), 80131 Naples, Italy
[3]ISPAAM, National Research Council, 80147 Naples, Italy

*These authors contributed equally to this work
‡Authors for correspondence (bonatti@unina.it; polish@tigem.it)

Accepted 18 June 2013
Journal of Cell Science 126, 4160–4172

doi: 10.1242/jcs.125443

Summary

The α-crystallin B chain (CRYAB or HspB5) is a cytosolic chaperone belonging to the small heat shock protein family, which is known to help in the folding of cytosolic proteins. Here we show that CRYAB binds the mutant form of at least two multispan transmembrane proteins (TMPs), exerting an anti-aggregation activity. It rescues the folding of mutant Frizzled4, which is responsible for a rare autosomal dominant form of familial exudative vitreoretinopathy (Fz4-FEVR), and the mutant ATP7B Cu transporter (ATP7B-H1069Q) associated with a common form of Wilson's disease. In the case of Fz4-FEVR, CRYAB prevents the formation of inter-chain disulfide bridges between the lumenal ectodomains of the aggregated mutant chains, which enables correct folding and promotes appropriate compartmentalization on the plasma membrane. ATP7B-H1069Q, with help from CRYAB, folds into the proper conformation, moves to the Golgi complex, and responds to copper overload in the same manner as wild-type ATP7B. These findings strongly suggest that CRYAB plays a pivotal role, previously undetected, in the folding of multispan TMPs and, from the cytosol, is able to orchestrate folding events that take place in the lumen of the ER. Our results contribute to the explanation of the complex scenario behind multispan TMP folding; additionally, they serve to expose interesting avenues for novel therapeutic approaches.

Key words: sHsp, Frizzled4, ATP7B

Introduction

To function properly, a protein must fold correctly. In addition to creating the right environment for the folding process, the cell engages a set of specialized chaperones that help the nascent chains attain native state by reducing the energy barriers they must overcome in order to fold correctly (Vabulas et al., 2010). Cellular chaperones play a crucial role in the proteostasis network (PN), the coordinated pathways of synthesis, folding, degradation and trafficking that take care of the overall protein homeostasis in the cell. Much effort is dedicated to finding ways to target the PN in order to develop therapeutic perspectives for a wide range of diseases that are linked to defective protein folding and trafficking (Hartl et al., 2011; Roth and Balch, 2011).

Due to their complex structure and topology, TMPs and, even more so, multispan TMPs have to overcome huge energy barriers in order to reach their native conformation (Janovjak et al., 2004). Not surprisingly, a number of human hereditary pathologies are linked to the loss of function of mutated TMPs (receptor, channel, pump or transporter), which then fail to attain native configuration (Hartl et al., 2011; Hung and Link, 2011). In some cases, these folding mutations primarily affect the transport of the TMPs but do not completely abolish the biological activity; thus the rescue of their proper localization could, in itself, significantly ameliorate the pathological consequences (Coppinger et al., 2012; Hung and Link, 2011).

Different categories of chaperone operate for TMPs, and the chaperone activity that is best characterized is of those located in the lumen of the ER (Braakman and Bulleid, 2011). However, cytosolic chaperones of the Hsp90, Hsp70 and Hsp40 families have been shown to assist in the folding of several TMPs by interacting with their cytosolic moiety and eventually causing different effects defined by the properties of each client protein (Beckmann et al., 1990; Marozkina et al., 2010; Mayer and Bukau, 2005; Peters et al., 2011).

Here we analyze the effect of a small Heat shock protein (sHsp), the α-crystallin B chain (CRYAB or HspB5) (Arrigo et al., 2007; Derham and Harding, 1999), which is a well known member of the sHsp family of 15–30 kDa. We show that this protein counteracts the aggregation and rescues the proper intracellular localization of two very different mutated multispan TMPs: the Frizzled4 (Fz4) receptor mutant L501fsX533 (henceforth referred to as Fz4-FEVR), associated with a rare form of Familial exudative vitreoretinopathy (FEVR); and the mutated copper (Cu) transporter ATP7B-H1069Q, associated with a common form of Wilson's disease (WD). This study was performed by expressing the exogenous CRYAB protein via trasfection in cells that lack this chaperone, but the main results were reproduced in cells that express the endogenous protein at the physiological level.

Journal of Cell Science

In Fz4-FEVR, a frameshift mutation (L501fsX533) generates a different and shorter C-terminal cytosolic tail of the receptor that accumulates in the ER of transfected cells (Robitaille et al., 2002). This misfolded mutant could potentially trap wild-type chains by improper heteroligomerization, thus abolishing Fz4 signaling from the cell surface during retinal development by a dominant negative mechanism (Kaykas et al., 2004). This loss of function results in aberrant vascularization of the retina during development, creating severe consequences for the patients (Gariano and Gardner, 2005; Ye et al., 2010).

In the ATP7B-H1069Q form of WD, the most frequent form among the Caucasian population (de Bie et al., 2007; Lutsenko et al., 2007; Payne et al., 1998), the mutated transporter accumulates in the ER of hepatocytes and, therefore, fails to reach the Golgi complex (as wild-type ATP7B) and to move further towards post-Golgi vesicles and the plasma membrane in response to increased cytosolic Cu level. This results in the failure to excrete excessive Cu out of the hepatocyte into the biliary flow, causing severe Cu toxicosis, which mainly affects hepatic and neurological functions (de Bie et al., 2007).

The possible molecular mechanism underlying the effect of CRYAB in the folding of Fz4-FEVR and ATP7B-H1069Q and the therapeutic perspectives opened by this new activity of CRYAB toward mutant multispan TMPs are subsequently discussed.

Results

CRYAB interacts with wild-type and mutant Fz4 forms

To identify the protein(s) interacting with the mutant Fz4-FEVR (Fig. 1A) we used a proteomic approach. N-terminally HA-tagged Fz4-FEVR was immunoprecipitated with anti-HA antibody from transfected HEK293 cells in order to then detect protein partners by nanoLC-ESI-LIT-MS/MS analysis. Consequently we detected CRYAB among the putative Fz4-FEVR interactors (supplementary material Table S1). This interaction was further confirmed by co-transfection of exogenous CRYAB (tagged at the N-terminus with 3×FLAG) with Fz4-FEVR cells followed by immunoprecipitation and immunoblotting, which clearly revealed that CRYAB was specifically co-immunoprecipitated by Fz4-FEVR (Fig. 1B). Interestingly, CRYAB was also co-immunoprecipitated by co-transfected Fz4 (Fig. 1B) and Fz4-Δ40 (a truncated form of Fz4 that bears only one residue of the predicted C-terminal cytosolic tail, supplementary material Fig. S1), indicating that CRYAB binds in the short cytosolic loops region of Fz4 and Fz4-FEVR, and not just to the new C-terminal tail of Fz4-FEVR generated by the frame-shift mutation (Fig. 1A). We then employed the proximity ligation assay (PLA) (Söderberg et al., 2008; Weibrecht et al., 2010), which allows for the detection and visualization of the close proximity between two proteins in tissue and cell samples using fluorescence microscopy. In this assay, a pair of oligonucleotide-conjugated secondary antibodies generates a DNA ligase-mediated fluorescent signal only when the primary antibodies against the corresponding proteins get close to each other. As a result, PLA signal was reported to indicate protein–protein interactions (Akbari et al., 2010; Weibrecht et al., 2010). To perform the PLA analysis we started with human hepatoma Huh-7 cells. These cells are larger and flatter than HEK293 cells, exhibit a well-defined and extended ER when observed with light microscopy (D'Agostino et al., 2011; Stornaiuolo et al., 2003), and do not express a detectable level of CRYAB (data not shown). Next, we generated a PLA-suitable mouse polyclonal antibody, specific for the cytosolic C-terminal tail of Fz4-FEVR. As shown in supplementary material Fig. S2, this antibody recognizes Fz4-FEVR (but not Fz4) in the immunofluorescence and western blot analyses performed on transfected cells and confirms that Fz4-FEVR was largely localized in the ER. When this antibody was employed in PLA experiments together with the anti-HA antibody in order to reveal transfected HA–CRYAB, a significant and diffuse PLA-associated staining was detected throughout the cells (Fig. 1C, upper panels), which clearly supported the above IP data that show an interaction between our proteins of interest. In the control experiment, as was expected, only background signal was generated when the anti-FLAG antibody was used instead of the anti-tail to detect Fz4-FEVR for PLA (Fig. 1C, central panels). This is because the 3×FLAG tag in Fz4-FEVR is located on the luminal side of the membrane with respect to the cytosolic HA–CRYAB protein. In addition, we employed the mutant G glycoprotein coded by the ts O45 strain of vesicular stomatitis virus (VSVG) as a further negative control. VSVG is a single-pass TM protein that accumulates in the ER at the non permissive temperature of 39℃ (Gallione and Rose, 1985; Kreis and Lodish, 1986). Therefore, cells were cotransfected with VSVG–GFP and HA–CRYAB and incubated at 39℃ to keep VSVG in the ER. As shown in Fig. 1C (lower panels), no staining was observed in the cells when an anti-GFP antibody (to reveal the C-terminus of VSVG) was employed in combination with the anti-HA (to label CRYAB) in the PLA assay. Taken together, the control experiments described above demonstrated the specificity of the PLA approach and also suggested that CRYAB binds to ER resident transmembrane proteins selectively. Unfortunately, we could not perform a similar analysis on the interaction of wild-type Fz4 with CRYAB due to the lack of a specific antibody recognizing the cytosolic portion of Fz4. Nonetheless, the above results strongly support the conclusion that CRYAB binds to Fz4 protein forms, which raises the interesting possibility that it may assist the folding of nascent Fz4 receptor chains.

CRYAB prevents the formation of large oligomeric complexes containing Fz4-FEVR

It has been reported that the Fz family receptor proteins form homo- and heteroligomers (Kaykas et al., 2004) and that the mutant Fz4-FEVR can trap wild-type chains in the ER in aberrant oligomers, thus explaining with a dominant negative mechanism the dominant inheritance of this mutation (Kaykas et al., 2004). Aberrant oligomerization may lead to the formation of incorrect inter-chains disulfide bonds (Marquardt and Helenius, 1992). Considering that 16 cysteine residues are present in the ectodomain and luminal loops of Fz4, the presence of incorrect disulfide bonds should be clearly recognizable in Fz4-FEVR using SDS-PAGE where the protein is run in non-reducing conditions. In the absence of DTT, the vast majority of Fz4-FEVR, but not of Fz4, migrated as high MW aggregates (Fig. 2A). In the presence of DTT, all apparent aggregates were converted to monomers, thus confirming their covalent nature (Fig. 2A). To further prove the aggregated nature of Fz4-FEVR, we analyzed the sedimentation profile on 20–40% glycerol gradients of Fz4 and Fz4-FEVR transfected in Huh-7 cells. As shown in Fig. 2B, wild-type Fz4 sedimented mostly in fractions 4 and 5, while Fz4-FEVR was additionally present in

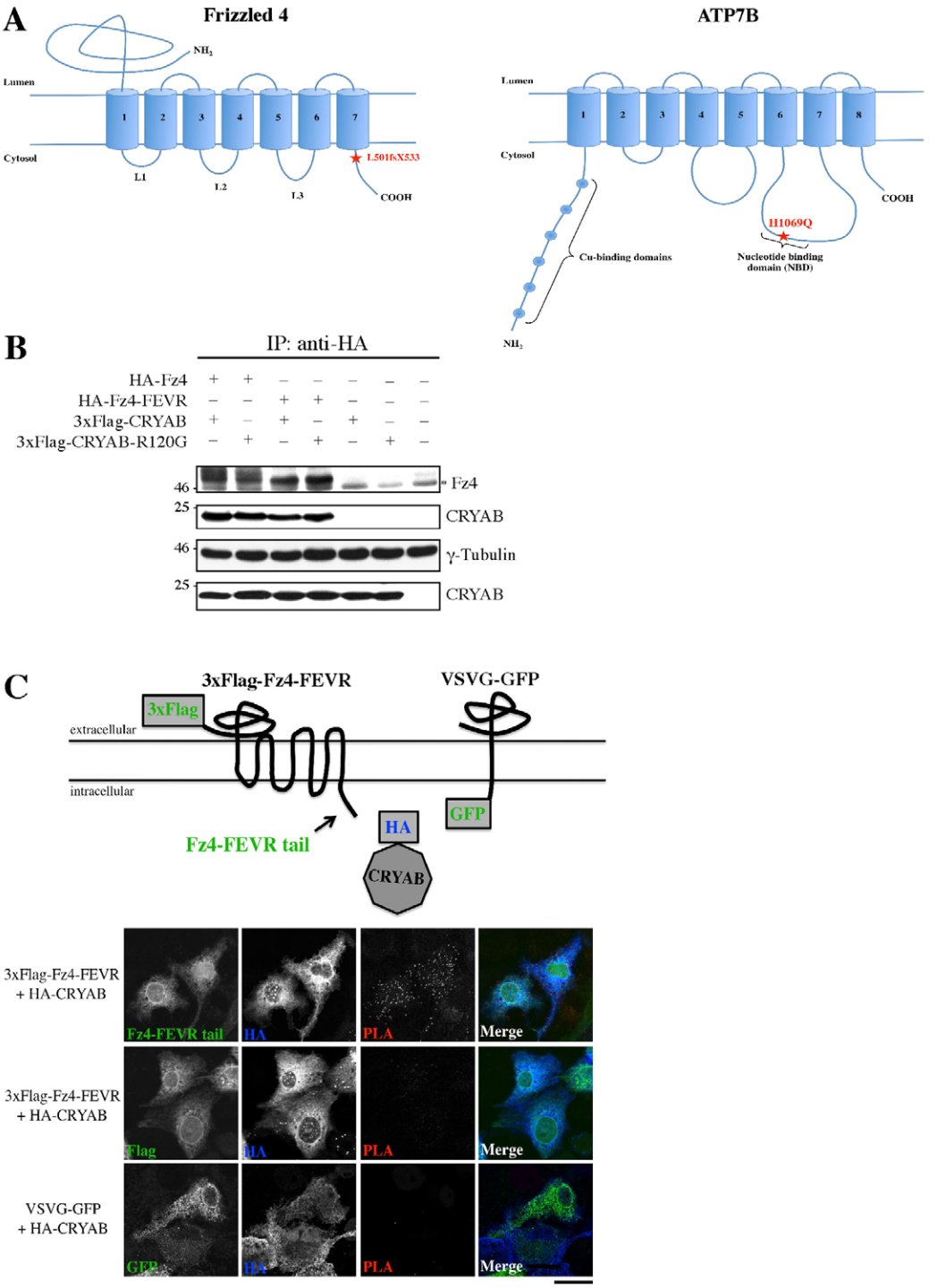

Fig. 1. Membrane topology of Fz4 and ATP7B and interaction between Fz4 and CRYAB. (A) Schematic drawing of Fz4 and ATP7B proteins. The star indicates the position of the frame-shift mutation that generates a different and slightly shorter C-terminal tail in Fz4-FEVR (36 residues instead of 41); and the position of the H1069Q mutation within the NBD of ATP7B. (B) HEK293 cells were transfected to express the tagged proteins indicated above the panels; detergent-lysed products immunoprecipitated by anti-HA antibody were analyzed by SDS-PAGE and immunoblotting as indicated on the right (in the top two panels). The bottom two panels show the immunoblotting of aliquots of the corresponding cell lysates. The asterisk indicates the migration of immunoglobulin heavy chain. The numbers on the left indicate the migration on the gel of M_r standards. (C) PLA analysis of the interaction between Fz4-FEVR and CRYAB. Plasmids expressing 3×FLAG–Fz4-FEVR and HA–CRYAB (see scheme) were co-transfected in Huh-7 cells and the assay was performed with the anti-Fz4-FEVR cytosolic tail or the anti-FLAG antibody together with the anti-HA antibody to detect CRYAB (top and middle rows, respectively). Given the flat shape of Huh-7 cells, confocal images were acquired with an open pinhole for better visualization of the overall volume of the cell. However, parallel *Z*-stacks analysis of thin confocal sections (1 Airy unit) excluded the presence of PLA signal from the nucleus (not shown). As a negative control, the assay was also performed with co-transfecting plasmids expressing GFP-tagged VSVG glycoprotein (see scheme) and HA–CRYAB, using anti-GFP and anti-HA antibodies (bottom row: see text for details). Scale bar: 10 μm.

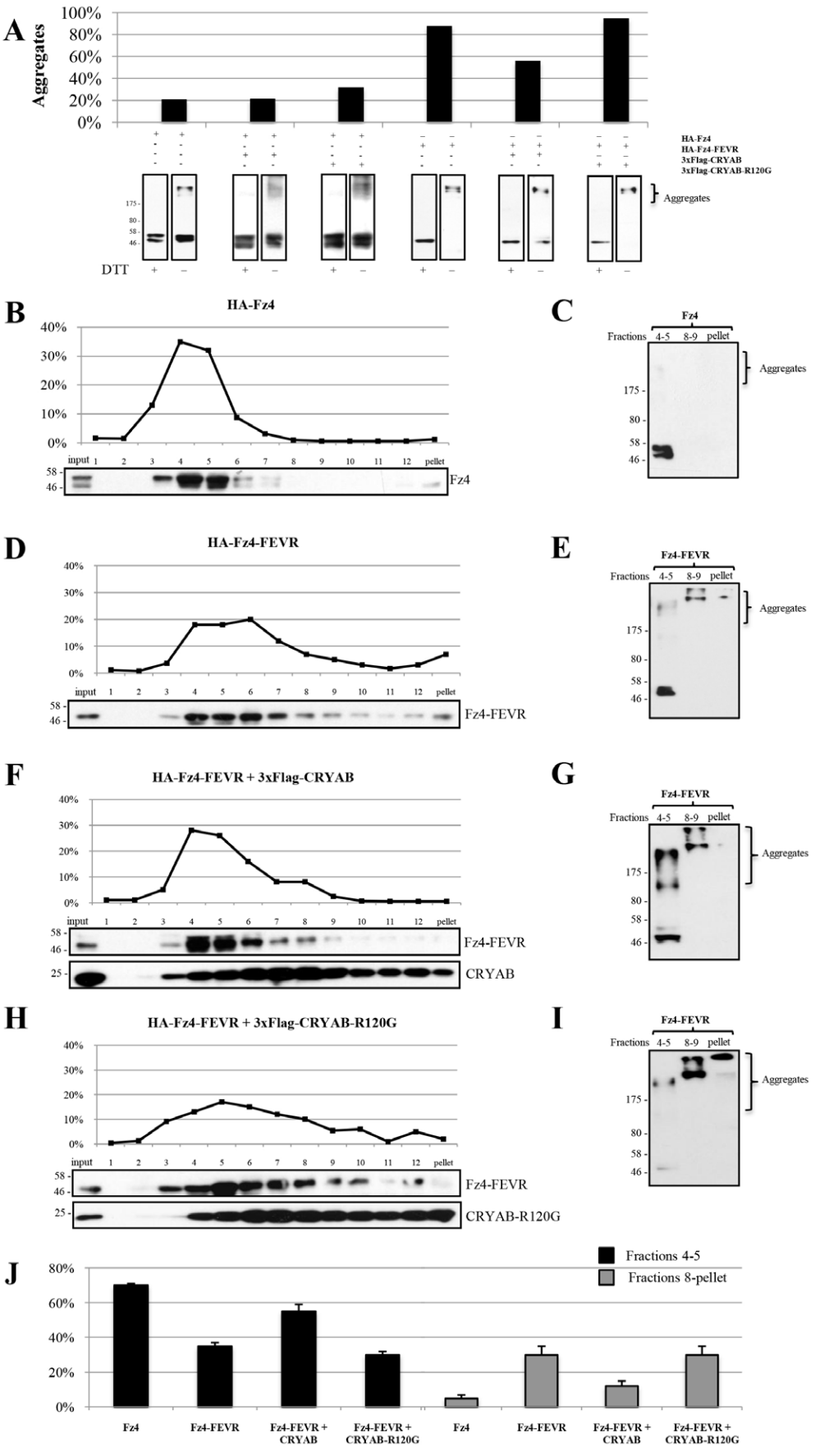

Fig. 2. CRYAB, but not CRYAB-R120G, reduces the amount of Fz4-FEVR oligomeric forms. (A) Huh-7 cells were transfected to express the tagged proteins indicated and equal aliquots of the cell lysates were processed in parallel for SDS-PAGE run in reducing (+ DTT) or non-reducing (– DTT) conditions followed by immunoblotting, in order to detect Fz4 or Fz4-FEVR. M_r on the left of the lower panels as in Fig. 1B and the position on the gels of the aggregated forms of Fz4 and Fz4-FEVR is indicated on the right. The histogram on top shows the percentage of the aggregated forms of Fz4 and Fz4-FEVR assessed with ImageJ software. (B,D,F,H) Huh-7 cells were transfected to express the tagged proteins indicated above the panels and aliquot of the cell lysates were analyzed on continuous 20–40% glycerol gradients (see the Materials and Methods for details). The collected fractions, and 1/20th of the total lysates (input), were analyzed by SDS-PAGE followed by immunoblotting that was developed with the antibodies indicated on the right side of the gels. Only the relevant part of the gels is shown. The percentage of Fz4 forms recovered in each fraction is indicated on the left side of the panels. (C,E,G,I) Aliquots of the indicated fractions from the gradient (shown in B,D,F,H, respectively) were analyzed on SDS-PAGE run in non-reducing conditions. (J) The amount of Fz4 or Fz4-FEVR (percentage of total) in light fractions 4–5 or heavy fractions 8–12 and in the pellet was calculated from the gradients shown in B,D,F,H (mean of two experiments ± s.d.).

large quantities in fraction 6 and in the lower part of the gradient, including the pellet fraction (Fig. 2D). The analysis of different regions of the gradient in non-reducing conditions showed that the Fz4 and Fz4-FEVR chains sedimenting in fractions 4–5 were mainly monomeric, while only high MW aggregates were present in fractions 8–9 and in the pellet (Fig. 2C,E). The quantification of these results showed that only about 5% of Fz4 sedimented from fraction 8 to the pellet, compared to 30% of Fz4-FEVR (Fig. 2J). Thus, the sedimentation profile of Fz4-FEVR with respect to Fz4 is very clear and indicates that Fz4-FEVR forms covalent aggregates that may reach a large size; however, the profile cannot tell if these are homo- or heteroligomeric aggregates.

To assess the effect of CRYAB on Fz4 and Fz4-FEVR, a similar analysis was performed on cell lysates co-transfected cells. No effect was observed for Fz4 (Fig. 2A), while the resultant amount of aggregated Fz4-FEVR was much lower than in the absence of CRYAB (Fig. 2A). On the glycerol gradient, the amount of Fz4-FEVR sedimented from fraction 8 to the pellet was about half of that observed in the absence of CRYAB (Fig. 2J) and almost no signal was detected in fractions 10–12 and in the pellet (Fig. 2F), which indicates that the larger aggregate containing Fz4-FEVR did not form. Interestingly, transfected CRYAB sedimented throughout nearly the entire gradient, including the pellet, with a peak centered in fractions 6 and 7 (Fig. 2F). This indicates, as expected, the formation of dimeric as well as oligomeric complexes (Ahmad et al., 2008).

To further test the hypothesis that the decreased aggregation of Fz4-FEVR was driven by the chaperone activity performed by CRYAB, we generated the CRYAB-R120G mutant by site directed mutagenesis (see methods). It is well established that this mutant binds to the client proteins but is largely defective in the chaperone activity (Bova et al., 1999; Zhang et al., 2010). Indeed, we found CRYAB-R120G specifically co-immunoprecipitated by either Fz4 or Fz4-FEVR (Fig. 1B); however, no effect was detected in preventing the aggregation of Fz4-FEVR in large oligomeric complexes (Fig. 2A,H and J), even though its own sedimentation profile was similar to wild-type CRYAB (Fig. 2F and H).

Given that the sedimentation analysis fully supported the anti aggregation hypothesis postulated above, we decided to challenge it with an entirely different approach. HA- and 3×FLAG-tagged versions of Fz4-FEVR were co-transfected in Huh-7 cells and their interaction *in situ* was analyzed with the PLA. As shown in Fig. 3, a strong signal, quantified as the number of spots per cell, was detected using anti-HA and anti-3×FLAG as primary antibodies, showing the close proximity of the two tagged Fz4-FEVR forms. Strikingly, when CRYAB was added to the co-transfection mix, the signal decreased to about one third of that scored in its absence (Fig. 3), which strongly suggested that CRYAB was efficiently blocking the heteroligomerization of the two reporters. Therefore, three completely different approaches supported the hypothesis asserting both the predisposition of Fz4-FEVR to form large aggregates and the property of CRYAB to specifically counteract the aggregation of Fz4-FEVR.

CRYAB rescues the cell surface expression of Fz4-FEVR

These results prompted us to investigate if the overexpression of CRYAB could rescue the intracellular transport of Fz4-FEVR toward the PM. As shown in Fig. 4A and B, Fz4 exhibited the same distribution when expressed in the absence or in the presence of co-transfected 3×FLAG–CRYAB, indicating that CRYAB does not impact the targeting of Fz4. Most of the Fz4 signal was detected on the PM (about 70% on average), while CRYAB was mostly distributed throughout the cytoplasm. The two proteins appeared not to co-localize. In contrast, Fz4-FEVR expressed alone was tightly located intracellularly, accumulating in the ER (Fig. 4D). However, when co-transfected with CRYAB (Fig. 4E), a significant amount of Fz4-FEVR was detected on the

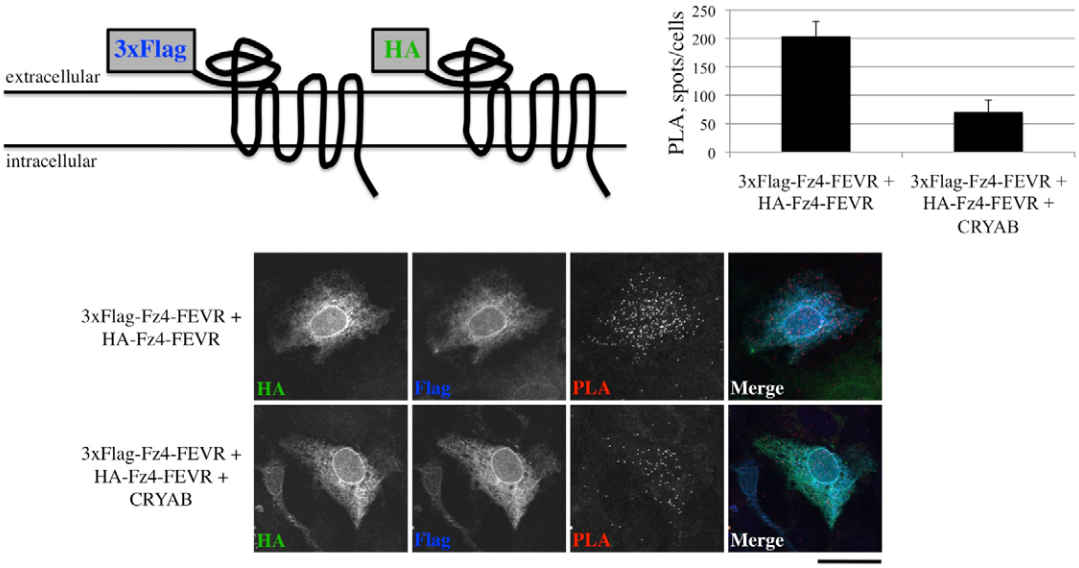

Fig. 3. CRYAB decreases heteroligomerization of differently tagged Fz4-FEVR forms. HA–Fz4-FEVR and 3×FLAG–Fz4-FEVR (see scheme) were co-transfected in Huh-7 cells in the absence or in the presence of co-transfected untagged CRYAB (top and bottom rows, respectively). The PLA analysis was performed with anti-HA and anti-FLAG antibodies. The histogram shows the number of PLA spots (means ± s.d.) counted in 30 cells randomly selected for the co-expression of the two Fz4-FEVR forms. Scale bar: 10 μm.

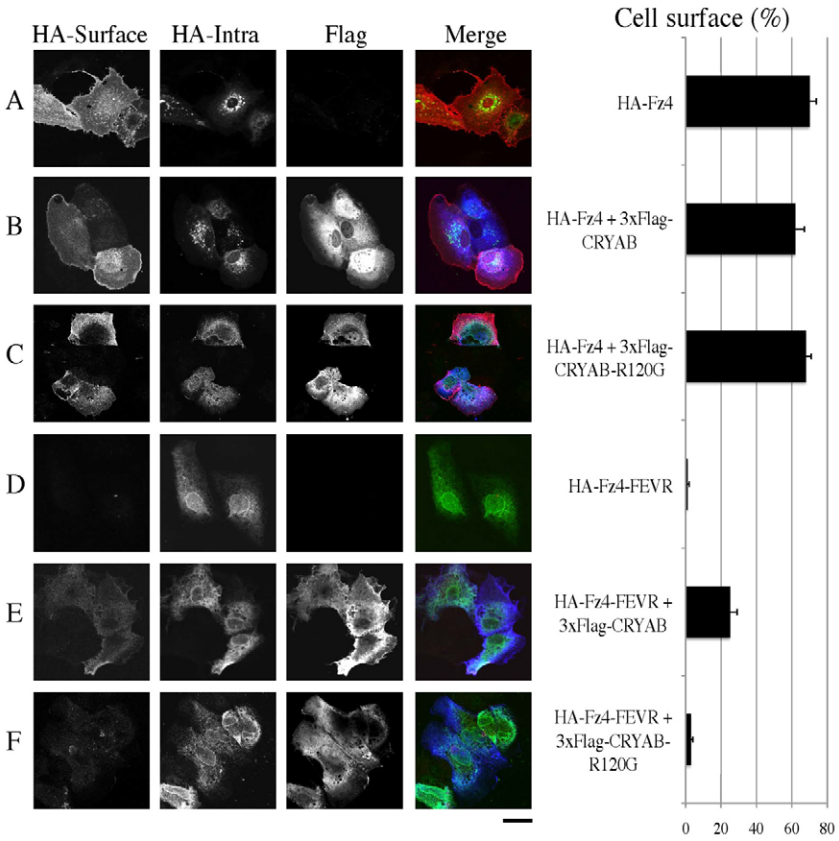

Fig. 4. CRYAB rescues cell surface expression of Fz4-FEVR. (A–F) Huh-7 cells grown on coverslips were transfected to express the tagged proteins indicated on the right. They were then processed for surface and intracellular staining of Fz4 and Fz4-FEVR (HA-Surface and HA-Intra), as detailed in the Materials and Methods, and were used to reveal, along with a third antibody against the FLAG tag, the transfected CRYAB or CRYAB-R120G. The histogram on the right shows the percentage of surface versus total staining (mean ± s.d., $n=20$ cells) for each condition. Scale bar: 10 μm.

cell surface (about 25% on average), while cells transfected with inactive CRYAB-R120G mutant exhibited a negligible amount of Fz4-FEVR on the cell surface (Fig. 4F). In control experiments no impact of CRYAB-R120G was observed on the distribution of Fz4 (Fig. 4C).

Finally, the rescue effect of CRYAB on the cell surface expression of Fz4-FEVR was challenged by incubating the cells in the presence of Brefeldin A (BFA). It is well established that BFA induces Golgi tubulation and fusion with the ER, thus blocking in the ER the protein destined to the PM (Cluett et al., 1993; Lippincott-Schwartz et al., 1989; Lippincott-Schwartz et al., 1990). As shown in supplementary material Fig. S3, no Fz4-FEVR was detected on the cell surface in cells co-transfected with Fz4-FEVR and CRYAB and incubated with BFA. This result rules out the possibility that CRYAB triggers the activation of unconventional secretory pathways from the ER to the PM (Gee et al., 2011). On the contrary, it suggests that CRYAB allows the newly synthesized Fz4-FEVR chains to reach the PM transiting through the Golgi complex.

CRYAB interacts with ATP7B and rescues the intracellular transport of WD-associated ATP7B-H1069Q mutant

In order to investigate whether CRYAB has a general role in assisting the folding of TMPs, we performed co-transfection experiments with other mutant TMPs that accumulate in the ER because they are misfolded/aggregated. Negative results were obtained with the mutant VSVG glycoprotein coded by the ts-045 strain; a minor, if any, effect was suggested by preliminary experiments with the P347S and D190G rhodopsin mutant (Li et al., 1996; Sung et al., 1991); and, as expected, CRYAB did not rescue ER-retained C150S or the C347G isoform of the GPI-anchored protein uromodulin since these mutants are not accessible from where CRYAB resides in the cytosol (data not shown). In contrast, CRYAB markedly recovered the intracellular compartmentalization of the H1069Q missense mutant of the Cu transporter ATP7B in COS-7 cells (Fig. 5). In line with previously reported evidence (Huster et al., 2003), we found almost 90% of the wild-type ATP7B (GFP-tagged at the N-terminus) in the late Golgi, where it overlapped with the TGN46 marker protein (Fig. 5). As reported (Huster et al., 2003), the similarly tagged ATP7B-H1069Q was firmly retained in the ER (Fig. 5), but more than 60% of the protein recovered the Golgi complex localization in the presence of co-transfected CRYAB (Fig. 5). As in the case of Fz4-FEVR, the chaperone activity-defective CRYAB-R120G hardly improved the ER localization of ATP7B-H1069Q (Fig. 5), and control experiments revealed no influence of both CRYAB and CRYAB-R120G on wild-type ATP7B compartmentalization (data not shown).

To further confirm the functional role of CRYAB in ATP7B-H1069Q rescue, the co-transfection experiments were repeated on a larger scale and ATP7B (or ATP7B-H1069Q) was immunoprecipitated from cell lysates. Fig. 6A shows that CRYAB (as well as CRYAB-R120G) was specifically pulled down by either ATP7B or ATP7B-H1069Q.

Next, we exploited the availability of multiple tools to visualize ATP7B-H1069Q (anti-GFP antibody to label the N-terminal portion of the GFP-tagged form, anti-nucleotide binding domain (NBD) antibody to visualize a more distal region of the protein, and the GFP tag itself to follow the distribution of the total protein) in order to study the interaction between CRYAB

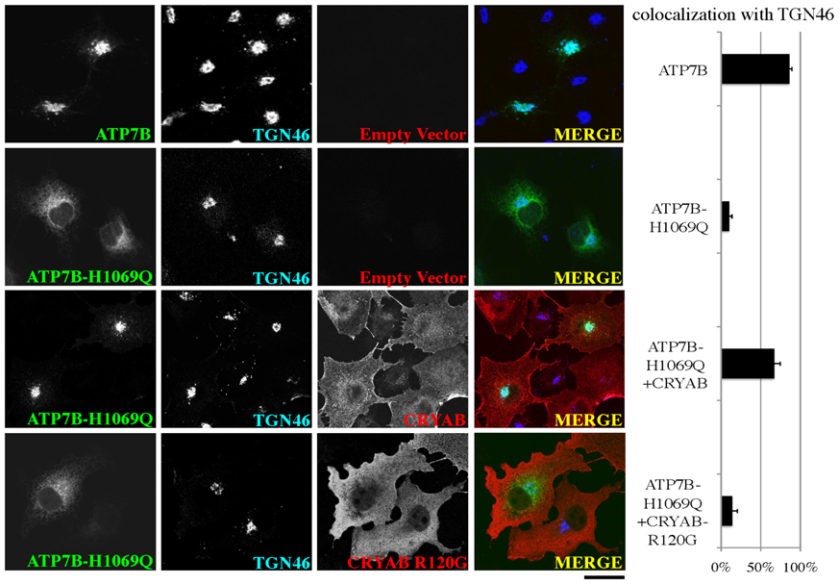

Fig. 5. CRYAB rescues Golgi complex localization of ATP7B-H1069Q. COS-7 cells grown on coverslips were transfected to express the tagged proteins indicated on the right side of each row and processed for immunofluorescence analysis using an anti-TGN46 protein antibody to visualize the Golgi complex. The histogram on the right shows the extent of colocalization (mean ± s.d.) of either ATP7B or ATP7B-H1069Q (visualized by GFP fluorescence) with TGN46. Scale bar: 10 μm.

and ATP7B-H1069Q with the PLA analysis. HeLa cells were selected to perform these experiments because they do not express endogenous ATP7B (unlike COS-7 and Huh-7 cells), thus the interaction of transfected ATP7B-H1069Q with CRYAB would not be contaminated by signals derived from the endogenous ATP7B. As shown in Fig. 6B (upper panels), a clear red fluorescent PLA signal indicated association of 3×FLAG–CRYAB with the NBD domain of ATP7B-H1069Q. Notably, this signal was never detected within the cells that did not exhibit any ATP7B-H1069Q fluorescence, which indicates, together with the negative control (see Materials and Methods), the specificity of the assay. Further analysis revealed the potential interaction of CRYAB with ATP7B-H1069Q to take place only in the peripheral regions of the cells (outside the Golgi). Moreover, the intensity of the PLA signal appeared to be lower in the cells where complete correction of ATP7B-H1069Q to the Golgi was achieved by CRYAB and appeared to increase in the cells where residual amounts of ATP7B-H1069Q were still visible in the ER. Therefore, the CRYAB–ATP7B-H1069Q interaction seems to occur mainly at the ER level. A similar, though even more intense, pattern was obtained using the anti-GFP antibody to detect the N-terminus of ATP7B-H1069Q (Fig. 6B, lower panels). The differing intensities of the two PLA signals most likely reflect the differing strengths of the two antibodies, or the closer proximity of the N-terminus of ATP7B-H1069Q to CRYAB. In any case, these results strongly suggest that a direct interaction occurs between CRYAB and ATP7B-H1069Q, and that this interaction takes place in the ER, the site where CRYAB is indeed expected to bind misfolded or aggregated TMP clients.

CRYAB eliminates the formation of large oligomeric complexes containing ATP7B-H1069Q

No information is available in the literature on the oligomerization status of ATP7B or its mutants, but it is known that a single chain may form the channel and excrete Cu ions (Lutsenko et al., 2007). Moreover, ATP7B has an opposite topology with respect to Fz4: it has no ectodomain, besides the short luminal loops that connect the transmembrane segments, and several cytosolic domains (Fig. 1A). Thus it is possible that CRYAB may employ a different mechanism to promote the transport of ATP7B-H1069Q from the ER. To address this question, we again used COS-7 cells and the glycerol gradient analysis. ATP7B sedimented mostly in fractions 5 and 6 but showed a clear shoulder in fractions 7 and 8 (Fig. 7A). In contrast, ATP7B-H1069Q sedimented mostly in fractions 6 and 7, with a shoulder in 8, and about 15% of the total was recovered in the pellet (Fig. 7B), which indicates the formation of large oligomeric complexes. Interestingly, in the presence of co-transfected CRYAB, these complexes were entirely absent and all the protein sedimented in fractions 6–9 (Fig. 7C). Most importantly, the presence of CRYAB-R120G had no effect in preventing the formation of these large oligomeric complexes recovered in the pellet (Fig. 7D), while both CRYAB and CRYAB-R120G also sedimented in COS-7 cells as dimeric as well as oligomeric complexes (Fig. 7C,D). Thus, CRYAB also exhibits evident anti-aggregation activity in the case of ATP7B-H1069Q.

The Golgi-corrected ATP7B-H1069Q moves to the cell surface in response to copper overload

It is well established that ATP7B resides in the Golgi complex under physiological conditions, but redistributes largely to Cu-excretion compartments (PM and associated post-Golgi vesicles) in the presence of elevated intracellular Cu concentration (La Fontaine and Mercer, 2007). This trafficking response of ATP7B is fundamental to the removal of excessive Cu away from the cell, thus preventing intoxication by Cu accumulation in the cytosol (La Fontaine and Mercer, 2007). To test whether ATPB-H1069Q, corrected to the Golgi by the activity of CRYAB, would also correctly respond to increasing Cu level, co-transfection experiments were performed in the human Hep-G2 hepatocytes, the liver-derived cellular system widely used to study ATP7B function (Cater et al., 2006; Roelofsen et al., 2000). Likewise the wild-type transporter, ATP7B-H1069Q rescued in the Golgi by CRYAB reached post-Golgi vesicles and the PM in cells incubated with 200 μM $CuSO_4$ (Fig. 8, compare the central panels of B and D, with A and C, respectively). In contrast, such

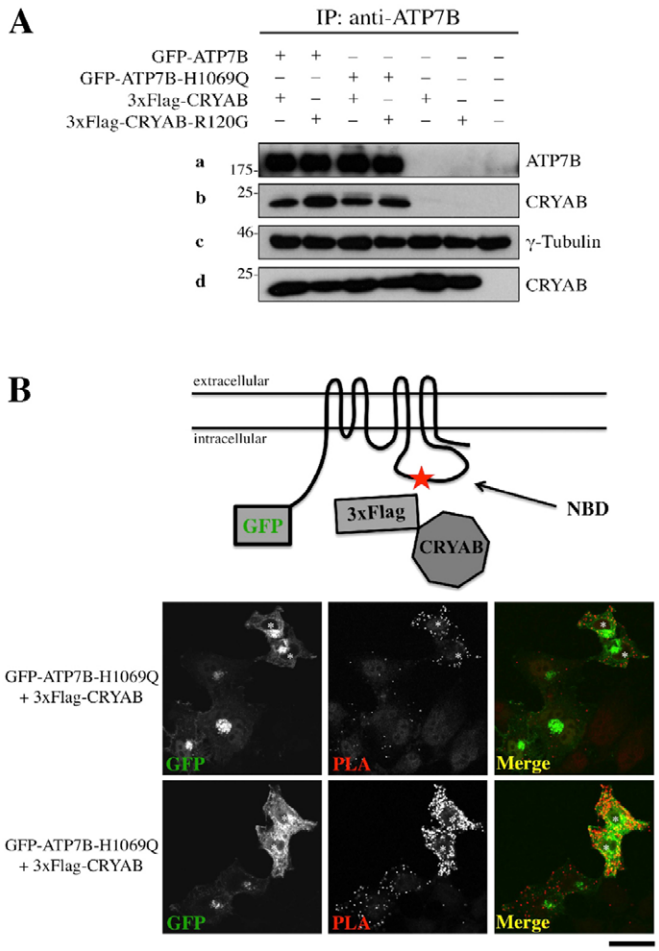

Fig. 6. Interaction between ATP7B and CRYAB. (A) COS-7 cells were transfected to express the tagged proteins (indicated above the panel), detergent-lysed, and the products were then immunoprecipitated by anti-GFP antibody. The results were analyzed by SDS-PAGE and immunoblotting, as indicated on the right side of the upper two panels. The lower two panels show the immunoblotting of aliquots of the corresponding cell lysates. Numbers on the left indicate M_r as in Fig. 1B. (B) PLA analysis of the interaction between GFP-tagged ATP7B-H1069Q and 3×FLAG–CRYAB. The two constructs (see scheme) were co-transfected in HeLa cells. The first image of each row shows the total distribution of ATP7B-H1069Q as revealed by GFP fluorescence; the second shows the PLA signal obtained with combinations of anti-ATP7B NBD and anti-FLAG antibodies (top row) or of anti-GFP and anti-FLAG antibodies (bottom row), respectively. The third image in each row shows the merge of GFP and PLA signals. Asterisks indicate the cells showing a higher level of residual ER staining of ATP7B-H1069Q. Scale bar: 10 μm.

Cu-dependent redistribution was not observed when ATP7B-H1069Q was expressed alone (Fig. 8E) or together with the mutant CRYAB-R120G (Fig. 8, compare the right panels of C and D). In all cases the mutant transporter remained in the ER. All of these results have been quantified (see the Materials and Methods), and are presented in the corresponding histogram (Fig. 8E). Overall, they strongly suggest that CRYAB allows ATP7B-H1069Q to traffic similarly to the wild-type ATP7B Cu pump.

Finally, we investigated whether the ATP7B-H1069Q, corrected to the Golgi by CRYAB, would have Cu excretion activity as in its wild-type counterpart. To this end, we used an assay based on a reporter luciferase enzyme that measures cytosolic Cu concentration (van den Berghe et al., 2007). Cells co-transfected with the control empty vector and above reporter exhibited a strong induction of luciferase in response to $CuSO_4$ (supplementary material Fig. S4). As expected, the expression of wild-type ATP7B significantly reduced the luciferase signal, which indicates that the pump was able to efficiently transport Cu away from the cytosol. Interestingly, ATP7B-H1069Q exhibited only a slightly lower capacity to eliminate Cu from the cytosol, regardless of whether the mutant was located in the ER, beyond the Golgi complex, or at the PM in the presence of CRYAB (supplementary material Fig. S5). Given that this residual activity would be sufficient to prevent the pathology if expressed in the right intracellular location (de Bie et al., 2007), CRYAB may open very interesting therapeutic perspectives on forms of WD that are due to ATP7BH1069Q.

Endogenous CRYAB corrects the compartmentalization of transfected ATP7B-H1069Q in COS-7 cells

Immunofluorescence analysis showed that a small minority of the COS-7 cells routinely grown in the lab expresses a detectable level of the endogenous CRYAB protein. As shown in supplementary material Fig. S5A, a weak signal was observed by western blot analysis compared to the exogenous transfected tagged-form (average transfection efficiency 30–40%), whereas no signal was detected in Hep-G2 (supplementary material Fig. S5B) and Huh-7 cells (data not shown). Thus we isolated, by limiting dilution, a variant COS-7 cell line (named COS-7/CRYAB+), in which the majority of the cells expressed significantly higher levels of endogenous CRYAB protein compared to parental cells (supplementary material Fig. S5B). When ATP7B-H1069Q was transfected in these cells, a clear CRYAB-dependent rescue of Golgi complex localization of the mutant transporter was observed (supplementary material Fig. S5C). The efficiency of the ATP7B-H1069Q rescue in COS-7/CRYAB+ cells appeared to be very close to that observed in the parental cells expressing exogenous 3×FLAG–CRYAB. This finding indicated that a massive overexpression of CRYAB was not required to correct the compartmentalization of ATP7B-H1069Q. Conversely, a moderate increase in endogenous CRYAB (which is still expressed about 10 times less than the transfected tagged-version) was sufficient to rescue the compartmentalization of ATP7B-H1069Q, even when this mutant was highly expressed upon transfection. This result further supported the use of CRYAB for therapeutic applications in this form of WD.

Discussion

Here we present compelling evidence that the cytosolic expression of CRYAB is able to rescue mutant Fz4-FEVR and ATP7B-H1069Q proteins from accumulation in the ER and, as a result, to power their intracellular transport to their final destination, where these proteins normally carry out their functions.

Two lines of evidence support the conclusion that CRYAB plays a direct role in this rescue: first, the specific co-immunoprecipitation (Fig. 1B and Fig. 6A) revealed either Fz4-FEVR or ATP7B-H1069Q to form a macromolecular complex with CRYAB; second, the specific signal obtained with the PLA analysis (Fig. 1C and Fig. 6B) strongly confirmed a possible interaction between CRYAB and each of the mutant TMPs, most

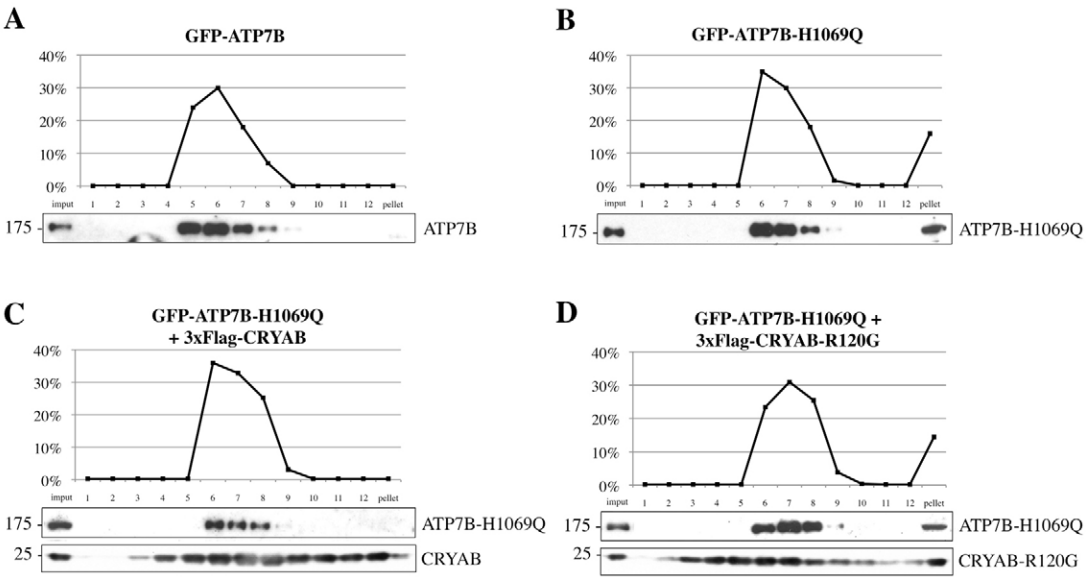

Fig. 7. CRYAB, but not CRYAB-R120G, eliminates the formation of large oligomeric complexes containing ATP7B-H1069Q. (A–D) COS-7 cells were transfected to express the tagged proteins (indicated above the panels) and aliquots of the cell lysates were analyzed on glycerol gradients as specified in Fig. 2.

likely occurring in the ER. This interaction results in a clear reduction of the amount of the aggregates containing Fz4-FEVR or ATP7B-H1069Q that form in the absence of CRYAB (Figs 2 and 7). This conclusion is derived from the sedimentation analysis performed by centrifugation in glycerol gradients and the SDS-PAGE analysis in non-reducing conditions, and is strongly supported by the finding that CRYAB-R120G, the chaperone-deficient mutant causing aberrant desmin folding and the consequent related myopathy (Bova et al., 1999; van Spaendonck-Zwarts et al., 2010; Wang et al., 2001), did not show any anti-aggregation activity. Moreover, the PLA analysis of differently N-terminally-tagged forms of Fz4-FEVR showed a strong reduction of aggregates in cells co-transfected with CRYAB (Fig. 3). Finally, and most importantly, the interaction with CRYAB and its anti-aggregation activity correlates with the rescue of plasma membrane and Golgi complex localization of Fz4-FEVR and ATP7B-H1069Q, respectively (Figs 4, 5 and supplementary material Fig. S5): both proteins are tightly localized in the ER either in the absence of CRYAB or in the presence of the mutant CRYAB-R120G. In addition, the Golgi-rescued ATP7B-H1069Q responded to Cu overload, similar to its wild-type counterpart, reaching post-Golgi vesicles and the plasma membrane (Fig. 8).

These results are very much in line with the main role ascribed to CRYAB: binding to cytosolic proteins and preventing their aggregation through an ATP-independent holdase activity (Arrigo et al., 2007; Kannan et al., 2012). Other features that distinguish the molecular function of CRYAB were also observed in our study. It has been reported that this sHsp (as well as other members of the family) forms large and dynamic homo- and hetero-oligomeric complexes that are instrumental in carrying out the holdase activity (Arrigo et al., 2007), and these CRYAB complexes were present both in Huh-7 and COS-7 transfected cells (Fig. 2). Moreover, the mutant CRYAB-R120G form maintains the binding activity and the ability to oligomerize, as expected (Bova et al., 1999). Lastly, our findings also support the view that CRYAB (as well as other members of its family) may favor with its holdase activity the function of other chaperones that assist in the folding of the clients, keeping it topologically ready for the folding machinery. To this end, we noted that the ability of CRYAB to recover the intracellular transport of Fz4-FEVR appears to be partially cell-dependent. A strong rescue effect was observed in Huh-7 and COS-7 cells, which was seen to be less intense in HeLa and weak in HEK293 cells; however, transfected CRYAB and Fz4-FEVR were both expressed at similar levels in all of the treated cell lines (data not shown), confirming that folding of Fz4 and transport from the ER does not depend exclusively on CRYAB. This conclusion is in full agreement with the current view, postulating that a large number of chaperones and other proteins work in a coordinated fashion towards the optimization of client protein folding, and to form cell specific proteostatis networks (Ong and Kelly, 2011; Roth and Balch, 2011).

Our working hypothesis is that CRYAB constitutively assists folding and post-folding events of Fz4 and ATP7B chains, though this activity is much more easily seen with their mutant forms. In the context of the proteostatic network view, extensive work will be needed to identify the members of the network that operate in conjunction with CRYAB for the folding of these proteins (Wang et al., 2006). At present, our results evince CRYAB to be a key component in such networks, but it will be interesting to investigate if HSP27 and other members of the sHsp family are endowed with the same activity towards TMPs that has been shown by CRYAB (Arrigo et al., 2007).

Our findings provide the important new evidence that CRYAB has additional client proteins among TMPs. This activity of CRYAB on TMPs, previously undetected, appears to be specific. No impact of CRYAB was detected on either the VSVG glycoprotein coded by the tsO45 strain at 39℃, or on the P347S and D190G rhodopsin mutants retained in the ER due to misfolding (de Silva et al., 1993; Li et al., 1996; Schnitzer et al., 1979; Sung et al., 1991) (data not shown). Most likely, since CRYAB is a chaperone, its specificity would be determined by the formation of misfolded protein aggregates apt to interact

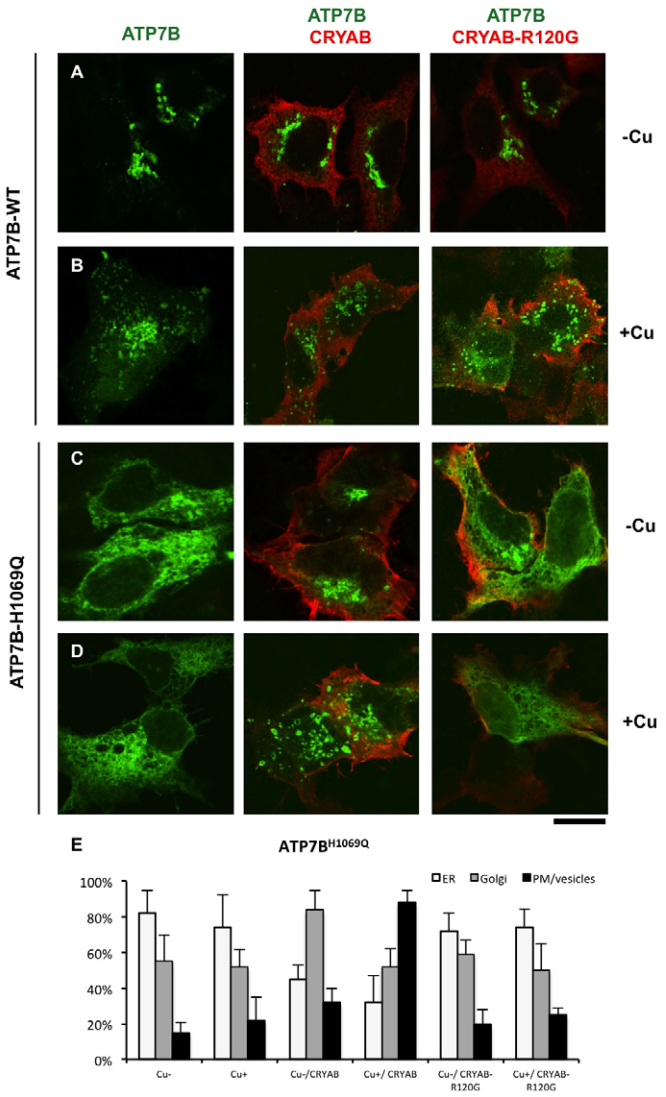

Fig. 8. ATP7B-H1069Q localized in the Golgi complex responds to Cu overload. Hep-G2 cells grown on coverslips were transfected with GFP-tagged ATP7B (A,B) or ATP7B-H1069Q (C,D) and co-transfected with 3×FLAG–CRYAB or CRYAB-R120G (as indicated above each column). Two days after transfection, parallel coverslips were incubated for 2 hours in medium containing either 200 mM $CuSO_4$ (+Cu) or 500 mM of the Cu chelant BCS (bathocuproinedisulfonic acid) (−Cu), and subsequently processed for immunofluorescence analysis. (E) Histogram showing the percentage of ATP7B-H1069Q-transfected cells exhibiting ER, Golgi complex, and plasma membrane and vesicular staining, respectively (mean ± s.d., $n=30$ fields from three independent experiments). Scale bar: 4.5 µm.

with CRYAB rather than by the recognition of specific aminoacidic sequences present in the misfolded protein. This hypothesis is better supported in the case of Fz4-FEVR, which has a much smaller mass exposed on the cytosolic side compared to the ATP7B protein. Fz4 cytosolic loops are short and presumably unstructured and site-directed mutagenesis of several residues has failed to abolish their interaction with CRYAB (data not shown). We predict that the new C-terminal tail of Fz4-FEVR could directly or indirectly disturb the correct interaction of the 7 transmembrane segments, thus generating a misfolded protein prone to aggregate. As a consequence, the ectodomains of adjacent chains exposed in the lumen of the ER would form inter-chain disulfide bridges, thereby stabilizing such aggregates. Noteworthy, neither ER retention nor aggregation are due to the high expression of Fz4-FEVR in transiently transfected cells as a HEK293 line permanently expressing Fz4-FEVR present the same phenotype (data not shown). It's interesting to note how clearly the binding of CRYAB, most likely to the cytosolic loops connecting the transmembrane domains, results in a beneficial effect on the luminal side of the chains, largely preventing the ectodomains to aggregate via disulfide bridges. We predict that chaperones in the lumen of the ER, yet to be identified, may concomitantly contribute to this effect.

How might CRYAB operate in the case of ATP7B-H1069Q correction? Our data suggest that CRYAB reduces oligomerization of this ATP7B mutant (Fig. 7). Unfortunately, little is known regarding ATP7B aggregation. This process may occur, since the third and fourth Cu-binding domains in the N-terminal portion of ATP7B have been shown to aggregate *in vitro* (Banci et al., 2008). Given that the H1069Q mutation might affect the strength of interaction between NBD and N-terminal domains of ATP7B (Dmitriev et al., 2011), the third and fourth Cu-binding domains in the N-terminal portion of the mutant ATP7B molecules could potentially acquire more freedom to oligomerise and generate ATP7B-H1069Q aggregates. CRYAB may counteract these aggregation events by holding the N-terminal tails of ATP7B-H1069Q molecules from oligomerization and in this way may help the mutant be exported from the ER. Further domain-specific analysis is needed in order to narrow down ATP7B and CRYAB binding sites and to fully understand the impact on ATP7B-H1069Q oligomerization. Both Fz4-FEVR and ATP7B-H1069Q are associated with human pathologies. As such, the unexpected effect of CRYAB opens interesting therapeutic perspectives. Fz4-FEVR is supposed to force wild-type Fz4 chain retention in the ER through hetero-oligomerization and, therefore, to suppress Fz4-mediated signalling at the cell surface during retinal development in a dominant-negative manner (Kaykas et al., 2004). ATP7B-H1069Q, in turn, is unable to efficiently reach the Golgi complex and to relocate to post-Golgi vesicles and the cell surface in response to Cu overload, thus failing to excrete Cu outside the cell. In the case of the rare form of FEVR associated with the mutant Fz4-FEVR, the assumption is that the protein corrected by CRYAB on the cell surface would be defective for signalling anyway, having lost the binding site for the Dishevelled protein in the mutated cytosolic tail (Krasnow et al., 1995; Tauriello et al., 2012). However, this correction should, at the same time, relocate wild-type Fz4 chains with fully functional signalling to the plasma membrane.

A more interesting scenario opens up for the CRYAB-mediated correction of the H1069Q variant of ATP7B that causes the most common form of WD. ER retention of ATP7B-H1069Q has been recognized as a main cause of toxic Cu accumulation in hepatocytes due to the failure of this mutant to transfer increasing Cu concentration through relocation towards Cu excretion sites (PM and associated post-Golgi vesicles) (de Bie et al., 2007). Meanwhile, a growing body of evidence suggests this mutant to possess significant catalytic activity (Iida et al., 1998; van den Berghe et al., 2009; our results). Therefore, ATP7B-H1069Q rescued from the ER to the intracellular compartments, where Cu excretion is executed by ATP7B, would be beneficial for a significant subset of WD patients. We

found that interaction with CRYAB facilitates ATP7B-H1069Q export from the ER towards the late Golgi compartment, in which ATP7B normally resides (Fig. 5), and CRYAB expression in hepatocytes allowed ATP7B-H1069Q delivery from the Golgi to the PM and associated vesicles upon addition of Cu (Fig. 8). Moreover, the endogenous CRYAB expressed in a variant COS-7 line is sufficient to rescue the Golgi localization of transfected ATP7B-H1069Q (supplementary material Fig. S5). Therefore, in the context of a clear demand for novel WD treatment strategies (Gitlin, 2003), CRYAB emerges as a new attractive therapeutic target as its upregulation in the liver may be beneficial for many patients and especially considering the H1069Q mutation of ATP7B is the most common cause of WD in the Caucasian population (de Bie et al., 2007; Lutsenko et al., 2007; Payne et al., 1998).

Finally, further work should be done with regard to mechanisms that modulate CRYAB expression in different tissues and organs given that it may have other disease-associated proteins as clients. Dexamethazone has already been shown to raise the expression of CRYAB (Aoyama et al., 1993; Jobling et al., 2001; Nédellec et al., 2002), thus providing an initial hint in this direction. Phosphorylation is reported to favor the formation of monomers/small oligomers of CRYAB that are less active with respect to the large oligomeric complexes fully endowed with holdase activity (Arrigo et al., 2007) over cytosolic targets. Specific protein kinase inhibitors (Aggeli et al., 2008; Hoover et al., 2000; Koppelman et al., 2008), or compounds targeting CRYAB phosphateses, may provide druggable components (Calamini et al., 2011) for the development of new therapeutic approaches, and perhaps cures, to a significant subset of genetic diseases by manipulating the proteostasis network (Balch et al., 2008; Lindquist and Kelly, 2011; Powers et al., 2009).

Materials and Methods

Reagents

All of the culture reagents were obtained from Sigma-Aldrich (Milan, Italy). The solid chemical and liquid reagents were obtained from E. Merck (Darmstadt, Germany), Farmitalia Carlo Erba (Milan, Italy), Serva Feinbiochemica (Heidelberg, Germany), Delchimica (Naples, Italy) and BDH (Poole, United Kingdom). Protein A-Sepharose CL-4B and the enhanced chemiluminescence reagents were from Roche (Milan, Italy).

Antibodies

The following antibodies were used: peroxidase-conjugated anti-mouse and anti-rabbit IgG, rabbit polyclonal anti-HA antibody and mouse monoclonal anti-FLAG antibody (Sigma-Aldrich, Milan, Italy); Texas-Red-conjugated anti-mouse and anti-rabbit IgG, FITC-conjugated goat anti-mouse and anti-rabbit IgG, Cy5-conjugated goat anti-mouse and anti-rabbit IgG (Jackson ImmunoResearch Laboratories, West Grove, PA); mouse monoclonal anti-HA antibody (Sigma Aldrich, Milan, Italy and Santa Cruz Biotechnology, Heidelberg, Germany); rabbit polyclonal anti-GFP (Abcam, UK); rabbit polyclonal anti-calnexin antibody (Stressgene, Ann Arbor, MI). A polyclonal antiserum against the cytosolic tail of Fz4-FEVR was generated by immunizing mice with the GST protein fused to the 36 residues of the C-terminal sequence of Fz4-FEVR. A polyclonal antibody against NBD of ATP7B was generously provided by Dr S. Lutsenko (John Hopkins Medical School, Baltimore, MD). A monoclonal antibody against human CRYAB was purchased from Santa Cruz Biotechnology (Heidelberg, Germany).

cDNA cloning and plasmid construction

The expression vectors pCDNA5/TO for Fz4 and the mutant L501fsX533 (Fz4-FEVR) are described above (D'Angelo et al., 2009). The expression vector pIRESpuro2-hFz4-c-myc was kindly provided by Guido J.R. Zaman (Verkaar et al., 2009). The expression vector pCMV6-XL5 for human CRYAB protein (ID NM_001885.1) was obtained from I.M.A.G.E. Consortium. To obtain the construct 3×FLAG–CRYAB, the cDNA coding for CRYAB was amplified from pCMV6-XL5 plasmid by PCR using the following oligos containing *Hin*dIII/*Xba*I flanking restriction sites and cloned into p3×FLAG–CMV-7.1: Fw (*Hin*dIII): 5′-AAGCTTATGGACATCGCCATCCACCACCC-3′; Rv (*Xba*I): 5′-TCTAGACTATTTCTTGGGGGCTGCGG-3′. To obtain the construct 3×FLAG–CRYAB (R120G) in which the R120 was substituted with a glycine (G), the construct 3×FLAG–CRYAB was used as a template and site direct mutagenesis was performed according to the manufacturer instructions (Roche) using the following oligos: Fw: 5′-CTCCAGGGAGTTCCACGGGAAATACCGGATCCCAG-3′; Rv: 5′-GTGGAACTCCCTGGAGATGAAACC-3′.

To obtain the construct HA–CRYAB, the cDNA coding for CRYAB was amplified from pCMV6-XL5 plasmid by PCR using the following oligos containing *Hin*dIII/XbaI flanking restriction sites and cloned into pCDNA3 expression vector (Invitrogen): Fw (*Eco*RI): 5′-GAATTCATGGACATCGCCATCCACCACCC-3′; Rv (*Xho*I): 5′-CTCGAGCTATTTCTTGGGGGCTGCGG-3′.

DNA of ATP7B and ATP7B-H1069Q GFP-tagged at the N-terminus was provided by Svetlana Lutsenko (John Hopkins Medical School, Baltimore, MD) and by Dominik Huster (Otto-von-Guericke-University, Magdeburg, Germany). DNA of VSVG protein with GFP-tag at its C-terminus was provided by Jennifer Lippincott-Schwartz (NICHD, NIH, Bethesda, MD). cDNA of transcription-based luciferase reporter (pGL3-E1b-TATA-4MRE) for measurement of cytosolic Cu was a generous gift from Bart van de Sluis (University Medical Center Groningen, Groningen, The Netherlands).

Cell culture, transfection and immunofluorescence

Cells were routinely grown at 37℃ in Dulbecco's modified essential medium (DMEM), containing 10% fetal bovine serum (FBS) and transfected using FuGene 6.0 (Roche, Milan, Italy), according to the manufacturer's instructions. The effect of CRYAB expression on the distribution of Fz4 or ATP7B protein forms was observed 48 hours post-transfection. Indirect immunofluorescence was performed as previously described (D'Agostino et al., 2011; Mottola et al., 2000). Single confocal images were acquired at 63× magnification on a LSM510 Meta or LSM710 confocal microscope (Carl Zeiss, Jena, Germany). To separately stain Fz4 protein forms on either cell surface or intracellular membranes, cells were incubated after fixation with rabbit polyclonal anti-HA antibody, briefly fixed again, and then permeabilized and incubated with mouse monoclonal anti-HA antibody. Two distinct secondary antibodies allowed separate visualization of the two fractions. Then, in order to measure the ratio between levels of PM and intracellular Fz4 protein forms, the immunofluorescence intensity in the two channels was measured using NIH ImageJ Biophotonic programs. For each co-transfection, 20 cells were considered for quantification. The results are given as mean ± s.d.

Preparation of cell extracts, immunoprecipitation SDS-PAGE and western immunoblotting

Preparation of cell extracts, immunoprecipitation SDS-PAGE, and western immunoblotting were performed as previously detailed (D'Agostino et al., 2011). Denaturation and reduction of Fz4 containing samples of SDS-PAGE was performed at 37℃ for 15 minutes.

Proximity ligation assay

In-situ protein-protein interactions, revealed as red fluorescent dots, were detected using the Duolink II PLAkit (Olink Bioscience, Uppsala, Sweden), according to the manufacturer's instructions. In the case of ATP7B, the antibody against the luminal domain of transferrin receptor (Invitrogen) was utilized as a negative control, given that this antibody should never link to either anti-GFP or anti-NBD antibodies, which reveal cytosolic regions of the transporter. In the experiments involving Fz4-FEVR, in order to visualize the distribution of the proteins expressed upon transfection, the samples were briefly fixed again after the PLA procedure and processed for immunofluorescence microscopy with the same couple of primary antibodies used previously and FITC and Cy5-conjugated anti-mouse and anti-rabbit IgG, respectively. Coverslips were mounted with Duolink Mounting Media containing DAPI nuclear stain and analyzed by confocal immunofluorescence microscopy, as detailed above.

Sedimentation analysis in glycerol gradients

Aliquots of cell extract obtained from transfected cells were loaded on top of 20–40% glycerol gradient made in lysis buffer (Tris-HCl 20 mM, NaCl 150 mM, Triton X-100 0.5%) and centrifuged at 4℃ in the Beckman SW-50.1 rotor for 16 hours at 45,000 rpm in a Beckman Coulter Optima L90K ultracentrifuge. Twelve fractions were collected from the bottom and the pellet was recovered in 0.3 ml of same lysis buffer used for glycerol gradient preparation. Aliquots of each fraction were analyzed by SDS-PAGE and immunoblotting.

Acknowledgements

We thank Guido Zaman for the myc-tagged Fz4 expression plasmid, Svetlana Lutsenko for ATP7B and ATP7B-H1069Q expression plasmids and for the anti-NBD antibody, Bart van de Sluis for the Cu

reporter, Gabriella Caporaso for her continuous support throughout the project, Massimo Mallardo and Alberto Auricchio for helpful discussions, and the TIGEM Advanced Microscopy and Imaging Core for microscopy support.

Author contributions

M.D., V.L., G.C., M.S., M.C.S., C.D., A.S., R.P. and S.B. conceived and designed experiments; M.D., V.L., G.C., M.S., M.C.S., C.D. performed experiments; M.D., V.L., G.C., M.S., M.C.S., C.D., A.S., R.P. and S.B. analyzed data; R.P. and S.B. wrote the manuscript.

Funding

This work was supported in part by Telethon grants [grant numbers GGP09029 to S.B. and TGM11CB4 to R.P.]; POR Campania FSE 2007–2013, Project CREME (to S.B.) and by an Italian Association for Cancer Research (AIRC) grant [grant number IG 10233 to R.P.]. G.C. was supported by a fellowship from POR Campania FSE 2007–2013, Asse IV.

Supplementary material available online at
http://jcs.biologists.org/lookup/suppl/doi:10.1242/jcs.125443/-/DC1

References

Aggeli, I. K., Beis, I. and Gaitanaki, C. (2008). Oxidative stress and calpain inhibition induce alpha B-crystallin phosphorylation via p38-MAPK and calcium signalling pathways in H9c2 cells. *Cell. Signal.* **20**, 1292-1302.

Ahmad, M. F., Raman, B., Ramakrishna, T. and Rao, C. M. (2008). Effect of phosphorylation on alpha B-crystallin: differences in stability, subunit exchange and chaperone activity of homo and mixed oligomers of alpha B-crystallin and its phosphorylation-mimicking mutant. *J. Mol. Biol.* **375**, 1040-1051.

Akbari, M., Solvang-Garten, K., Hanssen-Bauer, A., Lieske, N. V., Pettersen, H. S., Pettersen, G. K., Wilson, D. M., 3rd, Krokan, H. E. and Otterlei, M. (2010). Direct interaction between XRCC1 and UNG2 facilitates rapid repair of uracil in DNA by XRCC1 complexes. *DNA Repair (Amst.)* **9**, 785-795.

Aoyama, A., Fröhli, E., Schäfer, R. and Klemenz, R. (1993). Alpha B-crystallin expression in mouse NIH 3T3 fibroblasts: glucocorticoid responsiveness and involvement in thermal protection. *Mol. Cell. Biol.* **13**, 1824-1835.

Arrigo, A. P., Simon, S., Gibert, B., Kretz-Remy, C., Nivon, M., Czekalla, A., Guillet, D., Moulin, M., Diaz-Latoud, C. and Vicart, P. (2007). Hsp27 (HspB1) and alphaB-crystallin (HspB5) as therapeutic targets. *FEBS Lett.* **581**, 3665-3674.

Balch, W. E., Morimoto, R. I., Dillin, A. and Kelly, J. W. (2008). Adapting proteostasis for disease intervention. *Science* **319**, 916-919.

Banci, L., Bertini, I., Cantini, F., Rosenzweig, A. C. and Yatsunyk, L. A. (2008). Metal binding domains 3 and 4 of the Wilson disease protein: solution structure and interaction with the copper(I) chaperone HAH1. *Biochemistry* **47**, 7423-7429.

Beckmann, R. P., Mizzen, L. E. and Welch, W. J. (1990). Interaction of Hsp 70 with newly synthesized proteins: implications for protein folding and assembly. *Science* **248**, 850-854.

Bova, M. P., Yaron, O., Huang, Q., Ding, L., Haley, D. A., Stewart, P. L. and Horwitz, J. (1999). Mutation R120G in alphaB-crystallin, which is linked to a desmin-related myopathy, results in an irregular structure and defective chaperone-like function. *Proc. Natl. Acad. Sci. USA* **96**, 6137-6142.

Braakman, I. and Bulleid, N. J. (2011). Protein folding and modification in the mammalian endoplasmic reticulum. *Annu. Rev. Biochem.* **80**, 71-99.

Calamini, B., Silva, M. C., Madoux, F., Hutt, D. M., Khanna, S., Chalfant, M. A., Saldanha, S. A., Hodder, P., Tait, B. D., Garza, D. et al. (2011). Small-molecule proteostasis regulators for protein conformational diseases. *Nat. Chem. Biol.* **8**, 185-196.

Cater, M. A., La Fontaine, S., Shield, K., Deal, Y. and Mercer, J. F. (2006). ATP7B mediates vesicular sequestration of copper: insight into biliary copper excretion. *Gastroenterology* **130**, 493-506.

Cluett, E. B., Wood, S. A., Banta, M. and Brown, W. J. (1993). Tubulation of Golgi membranes in vivo and in vitro in the absence of brefeldin A. *J. Cell Biol.* **120**, 15-24.

Coppinger, J. A., Hutt, D. M., Razvi, A., Koulov, A. V., Pankow, S., Yates, J. R., 3rd and Balch, W. E. (2012). A chaperone trap contributes to the onset of cystic fibrosis. *PLoS ONE* **7**, e37682.

D'Agostino, M., Tornillo, G., Caporaso, M. G., Barone, M. V., Ghigo, E., Bonatti, S. and Mottola, G. (2011). Ligand of Numb proteins LNX1p80 and LNX2 interact with the human glycoprotein CD8α and promote its ubiquitylation and endocytosis. *J. Cell Sci.* **124**, 3545-3556.

D'Angelo, G., Prencipe, L., Iodice, L., Beznoussenko, G., Savarese, M., Marra, P., Di Tullio, G., Martire, G., De Matteis, M. A. and Bonatti, S. (2009). GRASP65 and GRASP55 sequentially promote the transport of C-terminal valine-bearing cargos to and through the Golgi complex. *J. Biol. Chem.* **284**, 34849-34860.

de Bie, P., Muller, P., Wijmenga, C. and Klomp, L. W. (2007). Molecular pathogenesis of Wilson and Menkes disease: correlation of mutations with molecular defects and disease phenotypes. *J. Med. Genet.* **44**, 673-688.

de Silva, A., Braakman, I. and Helenius, A. (1993). Posttranslational folding of vesicular stomatitis virus G protein in the ER: involvement of noncovalent and covalent complexes. *J. Cell Biol.* **120**, 647-655.

Derham, B. K. and Harding, J. J. (1999). Alpha-crystallin as a molecular chaperone. *Prog. Retin. Eye Res.* **18**, 463-509.

Dmitriev, O. Y., Bhattacharjee, A., Nokhrin, S., Uhlemann, E. M. and Lutsenko, S. (2011). Difference in stability of the N-domain underlies distinct intracellular properties of the E1064A and H1069Q mutants of copper-transporting ATPase ATP7B. *J. Biol. Chem.* **286**, 16355-16362.

Gallione, C. J. and Rose, J. K. (1985). A single amino acid substitution in a hydrophobic domain causes temperature-sensitive cell-surface transport of a mutant viral glycoprotein. *J. Virol.* **54**, 374-382.

Gariano, R. F. and Gardner, T. W. (2005). Retinal angiogenesis in development and disease. *Nature* **438**, 960-966.

Gee, H. Y., Noh, S. H., Tang, B. L., Kim, K. H. and Lee, M. G. (2011). Rescue of ΔF508-CFTR trafficking via a GRASP-dependent unconventional secretion pathway. *Cell* **146**, 746-760.

Gitlin, J. D. (2003). Wilson disease. *Gastroenterology* **125**, 1868-1877.

Hartl, F. U., Bracher, A. and Hayer-Hartl, M. (2011). Molecular chaperones in protein folding and proteostasis. *Nature* **475**, 324-332.

Hoover, H. E., Thuerauf, D. J., Martindale, J. J. and Glembotski, C. C. (2000). alpha B-crystallin gene induction and phosphorylation by MKK6-activated p38. A potential role for alpha B-crystallin as a target of the p38 branch of the cardiac stress response. *J. Biol. Chem.* **275**, 23825-23833.

Hung, M. C. and Link, W. (2011). Protein localization in disease and therapy. *J. Cell Sci.* **124**, 3381-3392.

Huster, D., Hoppert, M., Lutsenko, S., Zinke, J., Lehmann, C., Mössner, J., Berr, F. and Caca, K. (2003). Defective cellular localization of mutant ATP7B in Wilson's disease patients and hepatoma cell lines. *Gastroenterology* **124**, 335-345.

Iida, M., Terada, K., Sambongi, Y., Wakabayashi, T., Miura, N., Koyama, K., Futai, M. and Sugiyama, T. (1998). Analysis of functional domains of Wilson disease protein (ATP7B) in Saccharomyces cerevisiae. *FEBS Lett.* **428**, 281-285.

Janovjak, H., Struckmeier, J., Hubain, M., Kedrov, A., Kessler, M. and Müller, D. J. (2004). Probing the energy landscape of the membrane protein bacteriorhodopsin. *Structure* **12**, 871-879.

Jobling, A. I., Stevens, A. and Augusteyn, R. C. (2001). Binding of dexamethasone by alpha-crystallin. *Invest. Ophthalmol. Vis. Sci.* **42**, 1829-1832.

Kannan, R., Sreekumar, P. G. and Hinton, D. R. (2012). Novel roles for α-crystallins in retinal function and disease. *Prog. Retin. Eye Res.* **31**, 576-604.

Kaykas, A., Yang-Snyder, J., Héroux, M., Shah, K. V., Bouvier, M. and Moon, R. T. (2004). Mutant Frizzled 4 associated with vitreoretinopathy traps wild-type Frizzled in the endoplasmic reticulum by oligomerization. *Nat. Cell Biol.* **6**, 52-58.

Koppelman, B., Webb, H. K., Medicherla, S., Almirez, R., Feng, Y., Chavez, J. C., Mao, C. P., Nguyen, A., Liu, Y. W., Kapoun, A. M. et al. (2008). Pharmacological properties of SD-282 - an alpha-isoform selective inhibitor for p38 MAP kinase. *Pharmacology* **81**, 204-220.

Krasnow, R. E., Wong, L. L. and Adler, P. N. (1995). Dishevelled is a component of the frizzled signaling pathway in Drosophila. *Development* **121**, 4095-4102.

Kreis, T. E. and Lodish, H. F. (1986). Oligomerization is essential for transport of vesicular stomatitis viral glycoprotein to the cell surface. *Cell* **46**, 929-937.

La Fontaine, S. and Mercer, J. F. (2007). Trafficking of the copper-ATPases, ATP7A and ATP7B: role in copper homeostasis. *Arch. Biochem. Biophys.* **463**, 149-167.

Li, T., Snyder, W. K., Olsson, J. E. and Dryja, T. P. (1996). Transgenic mice carrying the dominant rhodopsin mutation P347S: evidence for defective vectorial transport of rhodopsin to the outer segments. *Proc. Natl. Acad. Sci. USA* **93**, 14176-14181.

Lindquist, S. L. and Kelly, J. W. (2011). Chemical and biological approaches for adapting proteostasis to ameliorate protein misfolding and aggregation diseases: progress and prognosis. *Cold Spring Harb. Perspect. Biol.* **3**, a004507.

Lippincott-Schwartz, J., Yuan, L. C., Bonifacino, J. S. and Klausner, R. D. (1989). Rapid redistribution of Golgi proteins into the ER in cells treated with brefeldin A: evidence for membrane cycling from Golgi to ER. *Cell* **56**, 801-813.

Lippincott-Schwartz, J., Donaldson, J. G., Schweizer, A., Berger, E. G., Hauri, H. P., Yuan, L. C. and Klausner, R. D. (1990). Microtubule-dependent retrograde transport of proteins into the ER in the presence of brefeldin A suggests an ER recycling pathway. *Cell* **60**, 821-836.

Lutsenko, S., Barnes, N. L., Bartee, M. Y. and Dmitriev, O. Y. (2007). Function and regulation of human copper-transporting ATPases. *Physiol. Rev.* **87**, 1011-1046.

Marozkina, N. V., Yemen, S., Borowitz, M., Liu, L., Plapp, M., Sun, F., Islam, R., Erdmann-Gilmore, P., Townsend, R. R., Lichti, C. F. et al. (2010). Hsp 70/Hsp 90 organizing protein as a nitrosylation target in cystic fibrosis therapy. *Proc. Natl. Acad. Sci. USA* **107**, 11393-11398.

Marquardt, T. and Helenius, A. (1992). Misfolding and aggregation of newly synthesized proteins in the endoplasmic reticulum. *J. Cell Biol.* **117**, 505-513.

Mayer, M. P. and Bukau, B. (2005). Hsp70 chaperones: cellular functions and molecular mechanism. *Cell. Mol. Life Sci.* **62**, 670-684.

Mottola, G., Jourdan, N., Castaldo, G., Malagolini, N., Lahm, A., Serafini-Cessi, F., Migliaccio, G. and Bonatti, S. (2000). A new determinant of endoplasmic reticulum localization is contained in the juxtamembrane region of the ectodomain of hepatitis C virus glycoprotein E1. *J. Biol. Chem.* **275**, 24070-24079.

Nédellec, P., Edling, Y., Perret, E., Fardeau, M. and Vicart, P. (2002). Glucocorticoid treatment induces expression of small heat shock proteins in human satellite cell populations: consequences for a desmin-related myopathy involving the R120G alpha B-crystallin mutation. *Neuromuscul. Disord.* **12**, 457-465.

Ong, D. S. and Kelly, J. W. (2011). Chemical and/or biological therapeutic strategies to ameliorate protein misfolding diseases. *Curr. Opin. Cell Biol.* **23**, 231-238.

Payne, A. S., Kelly, E. J. and Gitlin, J. D. (1998). Functional expression of the Wilson disease protein reveals mislocalization and impaired copper-dependent trafficking of the common H1069Q mutation. *Proc. Natl. Acad. Sci. USA* **95**, 10854-10859.

Peters, K. W., Okiyoneda, T., Balch, W. E., Braakman, I., Brodsky, J. L., Guggino, W. B., Penland, C. M., Pollard, H. B., Sorscher, E. J., Skach, W. R. et al. (2011). CFTR Folding Consortium: methods available for studies of CFTR folding and correction. *Methods Mol. Biol.* **742**, 335-353.

Powers, E. T., Morimoto, R. I., Dillin, A., Kelly, J. W. and Balch, W. E. (2009). Biological and chemical approaches to diseases of proteostasis deficiency. *Annu. Rev. Biochem.* **78**, 959-991.

Robitaille, J., MacDonald, M. L., Kaykas, A., Sheldahl, L. C., Zeisler, J., Dubé, M. P., Zhang, L. H., Singaraja, R. R., Guernsey, D. L., Zheng, B. et al. (2002). Mutant frizzled-4 disrupts retinal angiogenesis in familial exudative vitreoretinopathy. *Nat. Genet.* **32**, 326-330.

Roelofsen, H., Wolters, H., Van Luyn, M. J., Miura, N., Kuipers, F. and Vonk, R. J. (2000). Copper-induced apical trafficking of ATP7B in polarized hepatoma cells provides a mechanism for biliary copper excretion. *Gastroenterology* **119**, 782-793.

Roth, D. M. and Balch, W. E. (2011). Modeling general proteostasis: proteome balance in health and disease. *Curr. Opin. Cell Biol.* **23**, 126-134.

Schnitzer, T. J., Dickson, C. and Weiss, R. A. (1979). Morphological and biochemical characterization of viral particles produced by the tsO45 mutant of vesicular stomatitis virus at restrictive temperature. *J. Virol.* **29**, 185-195.

Söderberg, O., Leuchowius, K. J., Gullberg, M., Jarvius, M., Weibrecht, I., Larsson, L. G. and Landegren, U. (2008). Characterizing proteins and their interactions in cells and tissues using the in situ proximity ligation assay. *Methods* **45**, 227-232.

Stornaiuolo, M., Lotti, L. V., Borgese, N., Torrisi, M. R., Mottola, G., Martire, G. and Bonatti, S. (2003). KDEL and KKXX retrieval signals appended to the same reporter protein determine different trafficking between endoplasmic reticulum, intermediate compartment, and Golgi complex. *Mol. Biol. Cell* **14**, 889-902.

Sung, C. H., Davenport, C. M., Hennessey, J. C., Maumenee, I. H., Jacobson, S. G., Heckenlively, J. R., Nowakowski, R., Fishman, G., Gouras, P. and Nathans, J. (1991). Rhodopsin mutations in autosomal dominant retinitis pigmentosa. *Proc. Natl. Acad. Sci. USA* **88**, 6481-6485.

Tauriello, D. V., Jordens, I., Kirchner, K., Slootstra, J. W., Kruitwagen, T., Bouwman, B. A., Noutsou, M., Rüdiger, S. G., Schwamborn, K., Schambony, A. et al. (2012). Wnt/β-catenin signaling requires interaction of the Dishevelled DEP domain and C terminus with a discontinuous motif in Frizzled. *Proc. Natl. Acad. Sci. USA* **109**, E812-E820.

Vabulas, R. M., Raychaudhuri, S., Hayer-Hartl, M. and Hartl, F. U. (2010). Protein folding in the cytoplasm and the heat shock response. *Cold Spring Harb. Perspect. Biol.* **2**, a004390.

van den Berghe, P. V., Folmer, D. E., Malingré, H. E., van Beurden, E., Klomp, A. E., van de Sluis, B., Merkx, M., Berger, R. and Klomp, L. W. (2007). Human copper transporter 2 is localized in late endosomes and lysosomes and facilitates cellular copper uptake. *Biochem. J.* **407**, 49-59.

van den Berghe, P. V., Stapelbroek, J. M., Krieger, E., de Bie, P., van de Graaf, S. F., de Groot, R. E., van Beurden, E., Spijker, E., Houwen, R. H., Berger, R. et al. (2009). Reduced expression of ATP7B affected by Wilson disease-causing mutations is rescued by pharmacological folding chaperones 4-phenylbutyrate and curcumin. *Hepatology* **50**, 1783-1795.

van Spaendonck-Zwarts, K., van Hessem, L., Jongbloed, J. D., de Walle, H. E., Capetanaki, Y., van der Kooi, A. J., van Langen, I. M., van den Berg, M. P. and van Tintelen, J. P. (2010). Desmin-related myopathy: a review and meta-analysis. *Clin. Genet.* **80,** 354-366.

Verkaar, F., van Rosmalen, J. W., Smits, J. F., Blankesteijn, W. M. and Zaman, G. J. (2009). Stably overexpressed human Frizzled-2 signals through the beta-catenin pathway and does not activate Ca2+-mobilization in Human Embryonic Kidney 293 cells. *Cell. Signal.* **21**, 22-33.

Wang, X., Osinska, H., Klevitsky, R., Gerdes, A. M., Nieman, M., Lorenz, J., Hewett, T. and Robbins, J. (2001). Expression of R120G-alphaB-crystallin causes aberrant desmin and alphaB-crystallin aggregation and cardiomyopathy in mice. *Circ. Res.* **89**, 84-91.

Wang, X., Venable, J., LaPointe, P., Hutt, D. M., Koulov, A. V., Coppinger, J., Gurkan, C., Kellner, W., Matteson, J., Plutner, H. et al. (2006). Hsp90 cochaperone Aha1 downregulation rescues misfolding of CFTR in cystic fibrosis. *Cell* **127**, 803-815.

Weibrecht, I., Leuchowius, K. J., Clausson, C. M., Conze, T., Jarvius, M., Howell, W. M., Kamali-Moghaddam, M. and Söderberg, O. (2010). Proximity ligation assays: a recent addition to the proteomics toolbox. *Expert Rev. Proteomics* **7**, 401-409.

Ye, X., Wang, Y. and Nathans, J. (2010). The Norrin/Frizzled4 signaling pathway in retinal vascular development and disease. *Trends Mol. Med.* **16**, 417-425.

Zhang, H., Rajasekaran, N. S., Orosz, A., Xiao, X., Rechsteiner, M. and Benjamin, I. J. (2010). Selective degradation of aggregate-prone CryAB mutants by HSPB1 is mediated by ubiquitin-proteasome pathways. *J. Mol. Cell. Cardiol.* **49**, 918-930.